PLATE-MANTLE COUPLING AND CONTINENTAL FLOODING

Michael Gurnis

Department of Geological Sciences, The University of Michigan, Ann Arbor

Abstract. The flooding records of continents have been computed in dynamically self-consistent models of plates and convection. Platforms flood following rapid translation of continental plates as may occur following supercontinent breakup. In these models, continental flooding is primarily controlled by deep mantle sources and continental hypsometry is strongly influenced by dynamic topography. Some models, especially bottom heated ones, predict more extensive flooding than has been observed during the Phanerozoic. However, the computed flooding can be made consistent with the observations if: the viscosity of the upper regions of the convecting system are significantly reduced compared to the deep regions, the fluid is driven predominantly by internal heating, or the convection is confined to a depth appreciably less than the width of the non-subducting plate.

As continents move with respect to deep seated thermal anomalies and as the age distribution of sea floor evolves, the shape of the Earth changes. Such rearrangements of mantle buoyancy forces may have led to sea-level fluctuations of at least 200 meters amplitude over 10 to 100 million year time scales. Although a good case has been made for the correlation between the oceanic age distribution and flooding of continental platforms [Hays and Pitman, 1973], possible epeirogenic motion of continents caused by deep mantle anomalies remains conjectural [Bond, 1978]. The dynamic coupling between mantle and continents and the effect which such coupling could have on transgressions and regressions is unknown; the importance of deep seated mantle anomalies relative to shallow ones is also unknown. In this paper, some fundamental mantle controls on continental flooding have been explored with dynamically self-consistent numerical models of non-subducting plates interacting with thermal convection.

The primary observation constraining the dynamical models presented here is the Phanerozoic flooding record of continental platforms. During a major transgression, marine sediments are deposited on continental platforms; the area covered by such North American deposits has been compiled by Wise [1974]. After correcting for systematic trends, including the time interval between geologic maps, Wise [1974] showed that North America was never flooded by more than 30% during the Phanerozoic. The observed fraction now covered with marine deposits may underestimate the actual flooding because of erosion loss; this is particularly true for the Paleozoic record. One purpose of the present work is to find dynamic models consistent with observed flooding.

The two-way dynamic feedback between the motion of continental plates and mantle convection was explored by Gurnis [1988] with a two-dimensional finite element model.

This model was characterized by a thick non-subducting plate which was both more viscous and less dense than the surrounding fluid. Although low viscosity margins were placed on either side of the "plate", the bulk of the fluid had a uniform viscosity. The plate was pinned in a box of aspect ratio 8:1 with periodic boundary conditions. After applying a Galilean transformation using the mean horizontal velocity through the box, the plate was found to move episodically with respect to the bulk of the fluid. The thick plate inhibited the efficient cooling of the fluid beneath, such that a long wavelength thermal anomaly was established through the box. The plate repeatedly moved from hot upwelling to cold downwelling. In the present work, the single plate formulation of Gurnis [1988] has been extended to allow an investigation of continental flooding. The fundamental limitation of these models is that the top thermal boundary layer in the oceanic regions is not stiff, as they it is for the Earth, and therefore some fundamental physics could perhaps be missed.

Model Formulation

Infinite Prandtl number and incompressible convection is computed in a two dimensional rectangle with periodic boundary conditions using a finite element formulation [King, et al., 1990]. One node along the top is pinned (Figure 1a), while the remainder of the top and bottom surfaces are free slip. A high viscosity (η_c/η_o) and intrinsically buoyant (ρ_c/ρ_o) rectangle of total width, w_c, and depth, d_c, overlays the pinned node; this is the non-subducting plate. Low viscosity zones (η_w/η_o) are placed on the plate margins. The mean horizontal velocity through the box is V_0 and is an outcome of the computation. V_0 is used to transform the convecting system from "plate" centered to "mantle" centered.

The procedure used to determine flooding and sea-level changes is also summarized in Figure 1. Topography is the sum of both a dynamic and an isostatic component. The dynamic topography is determined from the solution of the fluid flow. Scaled topographies and geoids are within 1.5% of the values presented in a recent benchmarking effort [Blankenbach, et al. 1989]. To the dynamic topography, an isostatic topography was added to the area over the continental plate. The implicit cause of this topography is compensated crustal thickness variations. The isostatic topography follows the shape of the observed average of continental hypsometry [Harrison, et al., 1983]. A 5th order polynomial representation of this hypsometry (Figure 1b) is employed such that topography peaks at the continental center. All topographic heights and sea surfaces have been normalized by h_c, the height of the isostatic topography at the center of the plate (Figure 1b). On top of this dynamic and isostatic topography, a constant volume of ocean water was added such that isostatic compensation was always maintained; the water-surface was required to follow the geoid. The total volume of water added was such that the minimum fraction of flooding would be zero for the time interval analyzed. The final topography which results after water is isostatically balanced, was termed the total topography (Figure 1d). This procedure was applied to a time sequence of convection results.

The principle ambiguity of this model concerns the magnitude and shape of the imposed isostatic topography. The magnitude of isostatic topography, h_c, was adjusted so that the ratio between it and the topography in the oceanic areas, h_c/h_o,
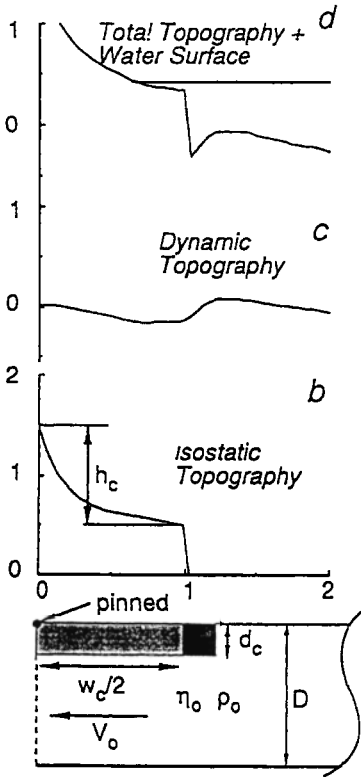
Fig. 1. Non-subducting plate (light shading) with margins (dark shading) embedded in the two-dimensional viscous region and b-d.) steps used in the computation of the total topography and water surface.

was in the same proportion as on the Earth. The primary drawback of this approach is that in the present models, h_O is strongly influenced by the upwelling and downwelling limbs [see Jarvis and Peltier, 1982]. For the Earth, h_O is apparently much more strongly controlled by the cooling of the lithosphere, as there is no convincing evidence for strong upwellings under ridges [Davies, 1988]. Furthermore, the isostatic hypsometry imposed on the models follows the topography actually observed for the continents, but observed topography is an unknown mixture of isostatic and dynamic components. This problem could be overcome if just enough isostatic topography was added such that the sum of the isostatic and dynamic components in the models matched the observed continental hypsometry. This latter approach was judged too complicated for these exploratory models.

Results and Discussion

Although a wide range of models have been investigated in which heating mode, Rayleigh number, aspect ratio, plate size, and other quantities have been systematically varied [Gurnis, manuscript in preparation], the fluid dynamics and flooding displayed the same general pattern of time dependence from case to case. In order to appreciate the behavior exhibited by these dynamic systems, three models are discussed. The results will be presented in three ways. First, Figure 2 shows a three-dimensional visualization of not only the two spatial and one time dimension but also shows the total topography and water-surface on the top. Second, Figure 3 shows the time history of continental parameters. Finally, time-evolving three-dimensional visualizations for the three cases have been recorded on the video, "Plate-mantle coupling and continental flooding". These animations are nearly identical to Figure 2 (see below and the caption to Figure 2)
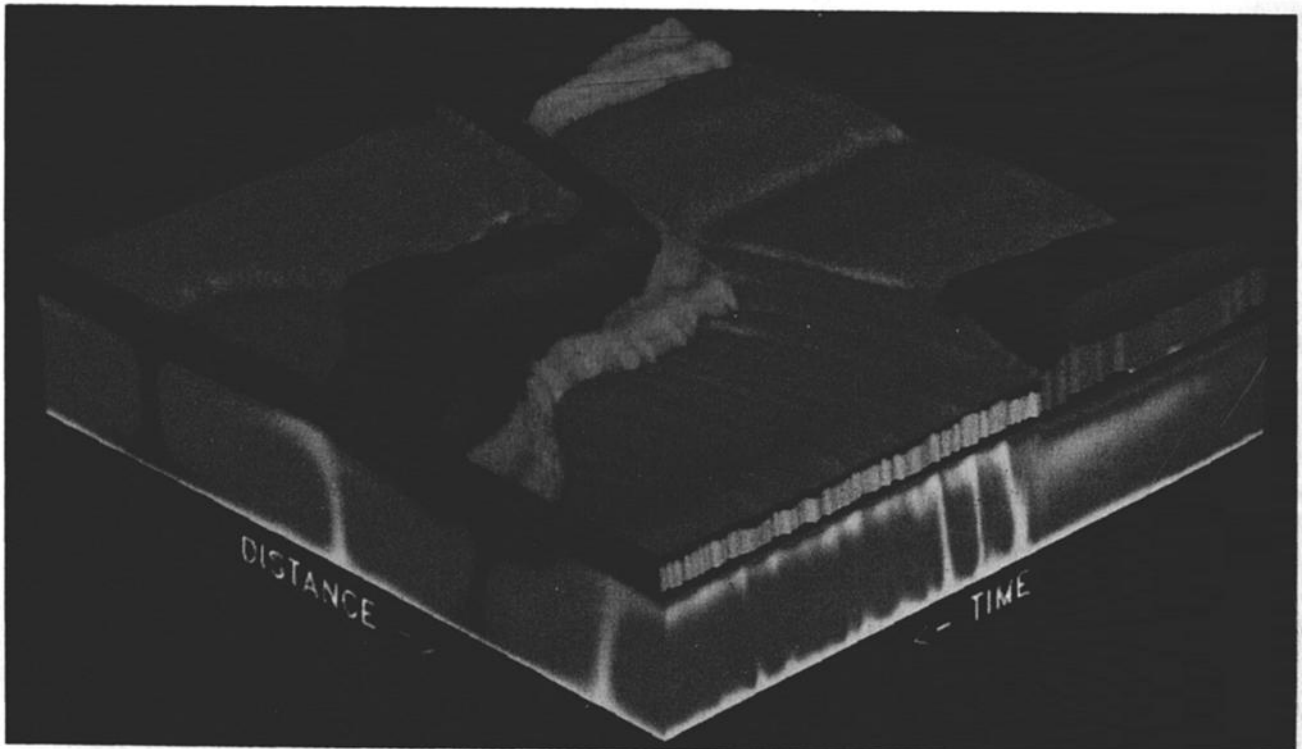

Fig. 2. Three-dimensional visualization of Case 1. The front vertical face is the temperature field at the end of the time sequence; the yellow fluid reaches a temperature of 1, while blue fluid reaches a temperature of 0. The side vertical face is the temperature field of a column which remains fixed with respect to the center of mass of the system. Time progresses from the back face (time=0.423) toward the front face (time=0.583). On the top surface the total topography and sea surface are displayed. One light illuminates the top from the upper right. The continental regions are green, the oceanic regions brown, and the water-surface is a transparent blue.
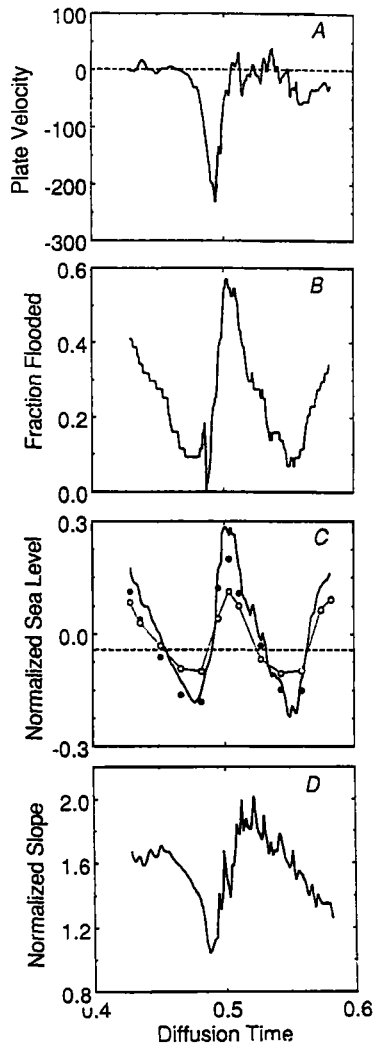
Fig. 3. Continental parameters as a function of diffusion time for Case 1: (a) plate velocity non-dimensionalized as a Peclet number; (b) fraction of continent flooded; (c) relative sea-level normalized by h_c; and (d) absolute value of the continental slope normalized by the slope of the purely isostatic component.

except that the front face continuously changes as time increases.

The first case considered is heated entirely from below. The fluid dynamical parameters of Case 1 are: Rayleigh number 10^5, box aspect ratio 6:1, viscosity of plate 10^3 (η_c/η_o), viscosity of margins 0.1 (η_w/η_o), and width of plate to box depth is 2:1 (w_c/D). Both the top and bottom surfaces were isothermal. The mesh had 33 nodes in the vertical and 129 in the horizontal directions. Our discussion will focus only on the latter part of the overall computation from diffusion time 0.429 to 0.583. Since the velocity and flooding displayed a repetitive behavior, we are able to concentrated our discussion on the final cycle of six total which occurred up to time 0.583; there was nothing special about this final cycle. As shown in Figures 2 and 3a, the continent remains stationary up to time 0.47; the continent remains pinned between two downwellings on the sides of the plate. On the time-depth face of Figure 2 (the vertical face to the right) one can see that the temperature under the plate increases. Initially there is a dominant downwelling close to the center of the "oceanic" region; this downwelling is evident in Figure 2 by the surface depression seen under the water surface. This downwelling is stationary like the plate. But at time 0.47 the continent moves laterally and comes to rest over this dominate downwelling

(video). The plate does not come perfectly to rest (Figure 3a), as the flow is now unsteady and characterized by frequent boundary layer instabilities. These boundary layer instabilities are evident in Figure 2 and on the video with the development of a "fish-bone" appearance in the total topography. This pattern is caused by the bowing down of the surface as the instabilities translate laterally toward the primary downwelling (video). The chaotic flow pattern is also evidenced by the crenelated pattern of the thermal structure on the time-depth face of Figure 2 and the erratic pattern of plate velocity after time 0.51 shown in Figure 3a.

During the initial period of zero plate velocity, the continent becomes progressively exposed (Figures 2 and 3b and on the video) and sea level drops with respect to the continent (Figure 3c). This exposure is caused by relative uplift of the continent as the temperature under the plate increases (right face, Figure 2). Continental flooding reaches a maximum of 55%, significantly larger than the observed 30% maximum [Wise, 1974]. The continent again becomes exposed as it remains approximately stationary. During and after this period of rapid translation, the continent not only moves vertically relative to the water surface, but it also changes shape (Figure 3d). During translation, the average slope of the continent decreases and reaches a minimum in slope during maximum plate velocity. The continent returns to a steeper slope when it comes to rest. These variations in continental hypsometry are consistent with movement over a dynamic topography low. It is evident, from the time varying magnitude of the continental slope (Figure 3d), that dynamic and isostatic topography play nearly equal roles, at least in Case 1 with a plate width:box depth ratio of 2:1.

In order to isolate the cause of this flooding, the lateral temperature contrasts within the upper 13% of the box (which was also the depth of the non-subducting plate, d_c) have been eliminated and the dynamic topography recomputed. The procedure described above has been followed to arrive at the total topography and relative sea level. These new sea levels (Figure 3c, solid circles) decrease by less than 20% from that which results from all of the buoyancy forces. Therefore, sea level must be primarily controlled by deep thermal anomalies (the upwelling and downwelling limbs of convection and the long wavelength thermal component) and not the top thermal boundary layer. This is not an entirely surprising result, considering that h_o is primarily controlled by the upwelling and downwelling limbs and not the simple thermal subsidence of the top thermal boundary layer.

Case 1 must be rejected because of the excessive amounts of flooding predicted: about 55% compared to a 30% maximum observed for the entire Phanerozoic. Extensive investigation of parameters shows that flooding can be reduced in a number of ways: by introducing a more realistic depth-dependent viscosity structure, by internally heating the convective system, or by increasing the plate width to box depth. Each of these will be discussed. It must be emphasized that stiffening up the top thermal boundary layers in the "oceanic" regions with a temperature-dependent viscosity will also have an effect on flooding; however, a more complicated formulation will be required to take this feature into account.

Decreasing the viscosity under the surface boundary layer mutes the dynamic topography from buoyant sources below such a low viscosity zone [Robinson, et al., 1987] and may lead to lower amplitude sea level fluctuations. For Case 1, the viscosity of the region between a depth 0.13 (the plate depth) and 0.5 has been reduced to 0.038, while the viscosity below 0.5 is increased to 11.3; these values were chosen because the average viscosity remains constant while giving a viscosity contrast of 300. This procedure is not self consistent, but allows a quick exploration of the role of deep viscosity. Dynamic topography has been recomputed and continent and oceans added. The total sea level fluctuations have been reduced by about 50% (open circles, Figure 3c). This easily reduces the flooding to less than 30%.

The role of internal heating is explored in Case 2 which is heated 80% from within and 20% by an isothermal bottom boundary condition. The effective Rayleigh number based on the transported heat is 7.6×10^4. All other features of Case 2 are identical as those in Case 1: box aspect ratio (6:1), plate width (2:1), and plate depth (0.13). The physics is similar to the bottom heated system; the primary difference is that prolonged periods of zero plate velocity are mostly absent, although plate velocity is still distinctly episodic (Figure 4a). Rapid flooding again follows the peak in plate velocity (Figure 4b; video). The primary difference from Case 1 is that flooding has been reduced to a 38% maximum compared to a 55% maximum. Again, the principal cause of these fluctuations are from deep anomalies, not shallow ones. The amplitude of flooding is reduced from the bottom heated case because of the absence of distinct upwelling limbs.
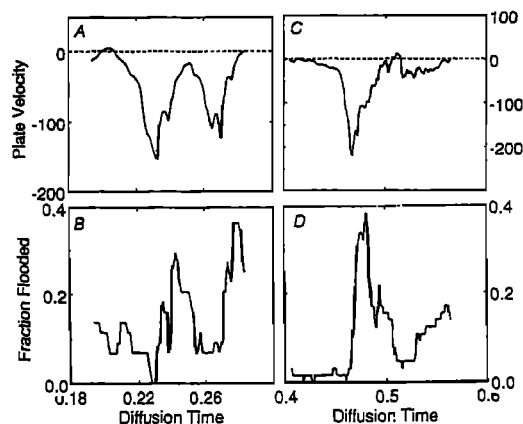

Fig. 4. Continental parameters as a function of time for Case 2: a.) plate velocity and b.) fraction of continent flooded. c-d) Same parameters for Case 3.

A factor influencing the amplitude of flooding is the ratio of plate width to the depth of the convecting region and this is explored in Case 3. Case 3 differs from Case 1 in that the plate aspect ratio has been increased from 2:1 to 4:1 and the box aspect ratio has been increased from 6:1 to 8:1 (the box size was increased to accommodate the larger plate). All other factors, including Rayleigh number, heating, and viscosity remain unchanged. Again a period of rapid flooding and then exposure follow the episode of lateral translation of the plate (Figure 4c,d; video), but flooding has been significantly reduced from 55% to 38%. The decrease in flooding with larger plates comes about because the aspect ratio of convection cells under the non-subducting plate; small plates can move from a single upwelling to a single downwelling, but larger plates overlay more than one upwelling limb and (or) more than one downwelling limb. The effect of a number of cells under a plate reduced the overall amplitude of flooding. Larger plates probably flood more in response to the long wavelength component of temperature variations within the interior of the fluid.

During rapid lateral translation, a thin thermal boundary layer replaces the non-subducting plate [Gurnis, 1988]. Thin thermal boundary layers develop in phase with the motion of a continent over a dynamic topography depression, but sea level changes not in response to this shallow structure but in response to deep structure. The computations highlight the possibility that increased spreading may be in phase with the motion of the continents over dynamic topography depressions. Since there is an observed correlation between platform flooding and ridge spreading since the Cretaceous [Hays and Pitman, 1973], epeirogenic motion of continents is not usually considered important in influencing sea level. These models show that increased ridge spreading could correlate with the motion of continents over lows in dynamic topography. This hypothesis could be tested when a more realistic formulation of oceanic areas is developed.

Conclusions

In summary, there are four primary conclusions. (1) If continents move with respect to deep thermal anomalies, a transgression and then a regression will follow a period of fast continental translation, as might occur after a supercontinent breakup. (2) In an iso-viscous system most of the flooding is caused by deep thermal anomalies. (3) The shape of continental hypsometry could be strongly influenced by dynamic topography; changes in hypsometry are in phase with sea-level oscillations. (4) The magnitude of flooding is strongly influenced by heating mode and plate width to box depth ratio.

References

Blankenbach, B. et al., A benchmark comparison for mantle convection codes, Geophys. J. 98, 23-38, 1989.
Bond, G., Speculations on real sea-level changes and vertical motions of continents at selected times in the Cretaceous and Tertiary Periods, Geology 6, 247-250, 1978.
Davies, G.F., Role of the lithosphere in mantle convection, J. Geophys. Res., 93, 10451-10466, 1988.
Gurnis, M., Large-scale mantle convection and the aggregation and dispersal of supercontinents, Nature. 332, 695-699, 1988.
Harrison, C. G. A., Miskell, K. J., Brass, G. W., Saltzman, E. S., and Sloan, J. L., Continental hypsography, Tectonics. 2, 357-377, 1983.
Hays, J. D. and Pitman, W.C., Lithospheric plate motion, sea-level changes and climatic and ecological consequences, Nature. 246, 18-22, 1973.
Jarvis, G.T. and W.R. Peltier, Mantle convection as a boundary layer phenomenon, Geophys. J. 68, 385-424, 1982.
King, S.D., A. Raefsky, and B.H. Hager, ConMan: Vectorizing a finite element code for incompressible two-dimensional convection in the Earth's mantle, Phys. Earth Planet. Int., in press.
Robinson, E. M., B. Parsons, and S.F. Daly, The effect of a shallow low viscosity zone on the apparent compensation depth of mid-plate swells, Earth Planet. Sci. Letts.. 82, 335-348, 1987.
Wise, D. U., Continental margins, freeboard and the volumes of continents and oceans through time, in The Geology of Continental Margins. (Edited by C.A. Burk and C.L. Drake), Springer-Verlag, New York, 45-58, 1974.

M. Gurnis, Dept. of Geological Sciences, University of Michigan, Ann Arbor, MI 48109-1063.